Colloids and Surfaces B: Biointerfaces 142 (2016) 214–222

Contents lists available at ScienceDirect

Colloids and Surfaces B: Biointerfaces

journal homepage: www.elsevier.com/locate/colsurfb

Delivery of fluorophores by calcium phosphate-coated nanoliposomes and interaction with *Staphylococcus aureus* biofilms

Ignacio Rivero Berti, María Laura Dell' Arciprete*, María Laura Dittler, Alejandro Miñan, Mónica Fernández Lorenzo de Mele, Mónica Gonzalez

Instituto de Investigaciones Fisicoquímicas Teóricas y Aplicadas, Facultad de Ciencias Exactas, Universidad Nacional de La Plata, Casilla de Correo 16, Sucursal 4, 1900 La Plata Argentina

ARTICLE INFO

Article history:
Received 25 November 2015
Received in revised form 22 February 2016
Accepted 1 March 2016
Available online 2 March 2016

Keywords:
Nanoliposomes
Calcium phosphate
Acridine orange
5, 10, 15, 20-Tetrakis(1-methyl-4-pyridinio)porphyrin
Staphylococcus aureus

ABSTRACT

The delivery capacity and mechanical stability of calcium phosphate (CaP) coated 1,2-dioleoyl-sn-glycero-3-phosphate (DOPA) liposomes free and adsorbed on bacterial surface was investigated introducing either acridine orange (AO) or 5,10,15,20-Tetrakis(1-methyl-4-pyridinio)porphyrin (TMP) in the aqueous core of the liposomes. The obtained nanomaterials were thoroughly characterized by electron and optical microscopy and by fluorescence techniques. Distribution of the AO and TMP molecules between the aqueous liposomes core and the outer solution was demonstrated by the band shifts and broadening of the excitation–emission matrices and the modified Stern-Volmer model for fluorescence quenching. In aqueous suspensions, c.a. 40% of AO was released to the outer solution while only a small percentage of TMP was observed to reach the outer liposome surface. The nanoliposomes adhesion capacity and the leaking of fluorophore molecules to *Staphylococcus aureus* (*S. aureus*) biofilms were further evaluated. A close interaction between liposomes and *S. aureus* biofilm was evidenced by TEM and SEM imaging. Epifluorescence experiments demonstrated that CaP-coated liposomes have good biofilm staining capability after two hours incubation of the biofilms with the liposomes, thus supporting an important release of the fluorophores when in contact with the biofilm. Altogether, the obtained results strongly suggest that CaP-coated liposomes are capable of activating drug release when in presence of *S. aureus* biofilms and smears. The studies herein presented, indicate that CaP-coated liposomes are potential vehicles for the selective delivery of drugs to *S. aureus* biofilms, as is the case of the singlet oxygen photosensitizer TMP, a well known photodynamic antibacterial agent.

1. Introduction

Liposomes carrying entrapped reporter molecules have been used in immunodiagnostics to provide signal amplification and to lower the detection limits of analytes [1]. Also, fluorescent dyes and quantum dots entrapped into hydrophilic lipid-based particles were developed as attractive targets for selective delivery of imaging agents to tumor cells [2,3]. The photophysical properties of encapsulated fluorophores are often regulated by the micellar structure improving the sensory capability of the dye [2,4]. Although liposomes promise the improvement of diverse abilities of the entrapped molecules [5], several drawbacks inherent to their structural assembling need being considered. Among the deficiencies of the lipid vesicles are the entrapped molecules leakage due to diffusion which results in a diminution of the efficiency [1], the liposome tendency to coalesce which turns their suspensions poorly stable, and the organic nature of their surface which converts them in labile structures [6]. In order to overcome these problems, coating with biocompatible and biodegradable substances such as polymers and calcium phosphate shells has been reported [7–12]. The calcium phosphate stoichiometry of the shell may be variable as the distinct phases are highly dependent on pH and the activity of ions in solution. As a consequence, they are denominated as CaP [9,13]. In particular, CaP-coated 1,2-dioleoyl-sn-glycero-3-phosphate (DOPA) liposomes have been reported as efficient nanoreactors for H_2O_2 sensing and drug delivery [9,14].

In the present study we assessed the potential ability of CaP-coated DOPA liposomes as vehicles for drug delivery in media inoculated with bacteria. To that purpose, the CaP-coated DOPA nanoliposomes were loaded with two extensively used dyes: acridine orange (AO) and 5,10,15,20-Tetrakis(1-methyl-4-pyridinio) porphyrin (TMP), Fig. 1. Acridine orange is a versatile and cell-

* Corresponding author.
E-mail address: mlaura@inifta.unlp.edu.ar (M.L. Dell' Arciprete).

http://dx.doi.org/10.1016/j.colsurfb.2016.03.003
0927-7765/

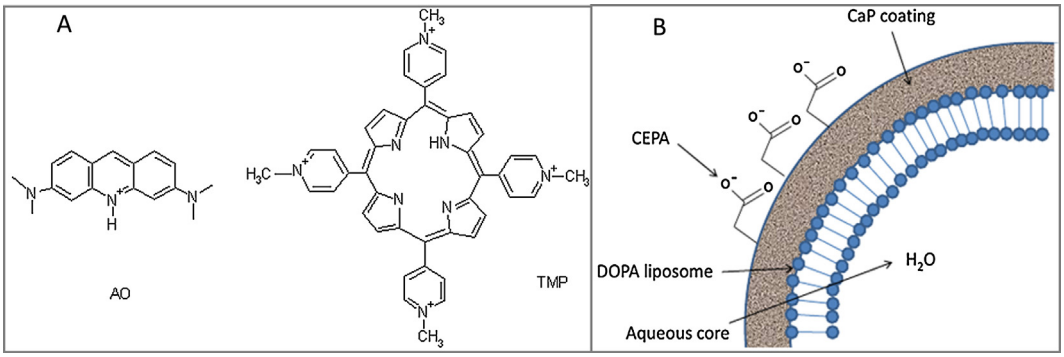

Fig. 1. (A) Acridine orange (left) and 5,10,15,20-Tetrakis(1-methyl-4-pyridinio) porphyrin(right) molecular structures. (B) Schematic view of the CaPLi nanoliposomes. (For interpretation of the references to color in this figure legend, the reader is referred to the web version of this article.)

permeable fluorescent dye which has been long and extensively used in fluorescence microscopy and flow cytometry analysis of cellular physiology and cell cycle status, and in the microscopic examination of microorganisms [15,16]. AO is adequate to stain planktonic bacteria, sessile cells, and biofilms. On the other hand, the water-soluble TMP is an efficient sensitizer of singlet oxygen [17,18] and therefore an efficient antimicrobial photodynamic agent [19]. The larger molecular size of TMP than that of AO allows the investigation of the effect of size on the diffusion of the fluorophores out of the CaP-coated liposome core.

Since *Staphylococcus aureus* (*S. aureus*) is one of the major worldwide pathogen causing community-acquired and nosocomial infections and its biofilms have been associated with poorer postsurgical outcomes [20,21], it was selected as a model of opportunistic pathogen target to evaluate the capability of CaP-coated liposomes as vehicles for the delivery of the encapsulated antimicrobial and staining fluorophores.

2. Experimental

2.1. Chemicals

1,2-Dioleoyl-sn-glycero-3-phosphate (DOPA) lipid was obtained as a lyophilized powder and stored at −18 °C until used (Avanti Polar Lipids). 2-Carboxyethyl phosphonic acid (CEPA)(94%,Sigma-Aldrich), glutaraldehyde (25%, Sigma −Aldrich) $CaCl_2$ (analitycal grade, Anedra), H_3PO_4 (85%,Cicarelli), NaCl (ACS,Anedra), NaOH (ACS, JTBaker), acetone (HPLC grade, Merck), glacial acetic acid (pro analysis, Merck), acridine orange (AO,Sigma, St Louis, MO, USA) and 5,10,15,20-Tetrakis(1-methyl-4-pyridinio) porphyrin (TMP,97%, Aldrich) were used without further purification. Regenerated cellulose dialysis tubing Spectra Por 1 with a MWCO of 6000–8000 Da was obtained from Spectrum Labs. A handheld extrusion apparatus with 100-nm polycarbonate (PC) filters (Millipore) was obtained from Avanti (Mini Extrusor 610000). Deionized water (>18 MΩ cm, <20 ppb of organic carbon) was obtained with a Millipore system.

2.2. Liposome synthesis

Liposomes were prepared by extrusion of 1 mL of 1 mg/mL DOPA lipid suspension in distilled water through a 100-nm PC filter at room temperature 11 times. The suspension contained alternatively AO (1×10^{-3} M) or TMP (1×10^{-4} M). After this procedure, the suspension became clear, indicating liposome assembly formation. In order to draw out the excess of AO or TMP, the solution was subsequently dialyzed against distilled water for 2 h and then overnight. DOPA liposomes are stable enough to act as a template for CaP nanoshells [10], as its negatively charged phosphatidyl groups assists the deposition of calcium ions around the vesicles [9].

2.3. Calcium phosphate (CaP) coating

CaP-coating of liposomes was performed following an adaptation of the method reported in the literature [9]. Freshly prepared 1 mL aqueous suspensions of liposomes and 100 μL of 0.1 M $CaCl_2$ were added to a 50 mL aqueous solution containing 10 μL of 1 M H_3PO_4 and 40 μL of 1 M NaOH (pH 10), while continuously stirring at 400 rpm. After 10, 30 or 120 min, 50 μL of 0.1 M CEPA was added to stop the CaP growth reaction. Subsequently, the suspension was stirred for additional 10 min, after which the samples turned opalescent. In order to eliminate the excess of AO and TMP, solutions were subsequently dialyzed against distilled water first for 2 h and then overnight. The resulting suspension was stored at 4 °C. The obtained samples were identified as: CaPLi, CaPLi-AO, and CaPLi-TMP, for CaP-coated DOPA liposomes with no added chromophore in the aqueous core, with added AO, and with added TMP, respectively.

Since the shell thickness was reported to depend on the elapsed reaction time of the synthesis mixture until CEPA addition [9], the thickness of the CaP shell capable of minimizing light scattering was optimized. To that purpose, the fluorescence intensity of CaPLi-AO particles as a function of the shell formation time was evaluated. Negligible emission was already observed after 30 min of CaP precipitation. Therefore, CEPA addition time was set to 10 min. During this period 40% of the initial emission is retained.

2.4. Bacterial suspensions and biofilm and smears formation

S. aureus (ATCC-25923) was inoculated in 150 mL of sterile liquid nutrient broth (Merck, Darmstadt, Germany) and grown for 24 h under gentle agitation at 37 °C until the optical density at 600 nm was greater than 1. Biofilms were prepared pouring 20 μL of bacterial suspension of OD = 1 over a glass slide which was incubated at 37 °C. After 2 h, the slides were washed with sterile water. 30 μL of CaP-Li AO suspension was poured over the biofilm. The liposomes were left to interact with the biofilm either for 15 min or 2 h at 37 °C. Then, slides were rinsed by immersion in a buffer solution. Alternatively, smears of planktonic culture were placed on a glass slide and 40 μL of 1:10 concentrated CaPLi-TMP were dripped over them and left to interact with the smears for 2 h at 37 °C prior to their observation.

2.5. Minimum inhibitory concentration determination

The Minimum Inhibitory Concentration (MIC) of AO, CaPLi-AO, TMP and CaPLi-TMP against S. aureus strain was determined by

the microtiter method as described in CLSI guidelines [22]. The assays were performed in triplicates and using independent bacterial cultures. The test was performed using 1:2 to 1:2048 serial dilutions and initial concentration of 1×10^{-3} M and 1×10^{-4} M for AO and TMP, respectively. In CaPLi-AO and CaPLi-TMP samples initial dyes concentration are on the order of 2×10^{-4} and 2×10^{-5} M, respectively.

2.6. Photophysical characterization techniques

UV–vis absorption measurements of the samples were performed using 10 mm bandpass quartz cuvettes in a Shimadzu 1800 series double beam spectrophotometer at a scan rate of 300 nm/min. *Photoluminescence measurements* were performed with a Jobin-Yvon Spex Fluorolog FL3-11 spectrometer equipped with a Xe lamp as the excitation source, a monochromator with 1 nm bandpass gap for selecting the excitation and emission wavelengths, and a red sensitive R928 PM detector. The spectra were corrected for the wavelength-dependent sensitivity of the detector while the source and the emission spectra were corrected for Raman scattering by using the solvent emission spectrum.

Luminescence lifetime and anisotropy measurements were performed by TCSPC (time correlated single photon counting) with LED excitation at 388 nm for TMP and CaPLi-TMP and 461 nm for AO and CaPLi-AO. Decays were recorded until 10,000 counts for AO containing samples and 2000 counts for TMP containing samples. Signal deconvolution was performed with a DAS 6.5HORIBA JobinYvon software. For anisotropy, the emission polarizer was set parallel and perpendicular to that of the excitation polarizer, from which the time dependent anisotropy r(t) is obtained. Generally, r(t) can be defined as a multi-exponential decay [23] from which the residual anisotropy (r_∞), the limiting anisotropy in the absence of rotational diffusion (r_0) and the individual correlation times ($\tau_{A,j}$) can be obtained. From the correlation times, the hydrodynamic radius (r_h) could be calculated using the Stokes-Debye–Einstein equation and considering spherical species [23].

The *electrophoretic mobility* of CaPLi- AO and CaPLi-TMP were measured with a Malvern NanoSizer (Nano-ZS) (UK). All the measurements were performed at 25 °C and in deionized water, with a cell drive voltage of 30 V using a monomodal analysis model.

2.7. Electron microscopy analysis

Transmission electron microscopy micrographs of CaPLi and *S. aureus* biofilm incubated with CaPLi-AO were taken with a JEOL JEM 1200 EX II microscope. Samples were prepared by dripping on carbon-coated 300-mesh copper grid and water evaporated in air. Alternatively the CaPLi sample was stained with 2% phosphotungstic acid. *Scanning electron microscopy* micrographs of CaPLi, *S. aureus* biofilm incubated with CaPLi-AO and CaP deposited in the absence of liposomes were taken using an environmental scanning electron microscope FEI Quanta 200. Sample preparation involved dehydration and fixation steps. Fixation was performed by immersion of the slides in a 2% glutaraldehyde solution at 4 °C for 2 h and washed with a buffer solution. Dehydration was performed by sequential immersion in cool ethanol-water mixtures (30%, 50%, 70%, 90% and 95%) followed by two immersion processes in absolute ethanol at room temperature for 20 min [24]. Samples were treated by critical point drying in order to replace the liquids by CO_2 and further metalized with Au. In order to study bacterial interactions, samples of *S. aureus* and *S. aureus* incubated with CaPLi-AO were treated and observed under similar conditions for comparison purposes.

Epifluorescence microscopy of both, biofilms and smears, were performed with a fluorescence microscope (Olympus BX51, Olympus Corp., Tokyo, Japan) equipped with a #WB filter, for AO and CaPLi-AO samples (dichroic mirror DM500, excitation filter BP450-480, emission filter BA515) and a #WG filter, for TMP and CaPLi-TMP samples (dichroic mirror DM570, excitation filter BP510-550, emission filter BA590). The microscope is connected to an Olympus DP71 (Olympus Corp., Tokyo, Japan) color video camera. Images were taken immediately after opening the microscope shutter to the computer monitor.

2.8. AO encapsulation efficiency

The percentage encapsulation efficiency (EE%) of AO and TMP in the liposomes was estimated from fluorescence emission experiments. The dye EE% was determined as the ratio between the maximum counts of uncovered liposomes, C_{lipo}, to those of the free aqueous fluorophore sample, C_{free}, at the maximum emission of the fluorophore, $EE\% = 100 \times C_{lipo}/C_{free}$. The calculation takes into consideration that the scattering of uncovered-liposome samples did no significantly affect the fluorescence measurements and the emission quantum yield is similar in both environments. The EE% obtained for AO is of 18%, in agreement with reported values for fluorescent dyes encapsulated by extrusion method with 100-nm PC filter [25]. For TMP the considerations may not be valid and EE% could not be calculated. The intensity emission of CaPLi-TMP sample is higher than that of free TMP solution giving rise to a meaningless result. The observation was previously reported and assigned to the increase in porphyrin fraction bound to the vesicles [26].

3. Results and discussion

3.1. Characterization and photophysical behavior of CaPLi containing entrapped dyes

3.1.1. TEM and SEM characterization

TEM micrographs in Fig. 2A show CaPLi as spherical dense objects with a heterogeneous population of sizes ranging from 200 nm to 400 nm. Phosphotungstic acid stained samples (Fig. 2A *inset*) show the internal structure of the vesicle with a distinctive core-shell structure. The thickness of CaP coating estimated from that figure is about 20–40 nm. Also, Fig. 2B displays a SEM micrograph of a spherical CaPLi vesicle with conserved shape. The mechanical stability gained by the coated liposomes is evidenced by the preserved form in SEM image, as the pretreatment involved a strong dehydration process. Rod-like particles observed in some SEM micrographs correspond to CaP crystal (see Supporting Material).

The electrophoretic mobility of CaPLi-AO $(-2.6 \pm 0.3) \times 10^{-4}\ cm^2\ V^{-1}\ s^{-1}$ and CaPLi-TMP $(-2.9 \pm 0.2) \times 10^{-4}\ cm^2\ V^{-1}\ s^{-1}$ are coincident within the experimental error. Therefore, considering average sizes independent of the nature of the enclosed fluorophore, CaPLi-AO and CaPLi-TMP vesicles show similar average surface charges. These observations support negligible fluorophore adsorption on the particles surface.

3.1.2. Photophysical characterization

In order to minimize the formation of AO dimmers and aggregates, [AO] $<10^{-3}$ M and pH solutions in the range from 2 to 8 were used throughout the experiments before CaP coating of liposomes. Dimmer and larger aggregates formation was controlled by their characteristic absorption at 465–450 nm [16,27–29]. Otherwise, AO cationic monomer shows maximum absorption at 492 nm. AO solutions show excitation–emission maxima (λ_{exc}/nm, λ_{em}/nm) at (495, 530) in agreement with reported values for the AO cation monomer [16,30]. On the other hand, CaPLi-AO suspension showed an excitation–emission maxima at (500, 535), 5 nm shifted to higher wavelengths with respect to free AO in solution (Fig. 3A).

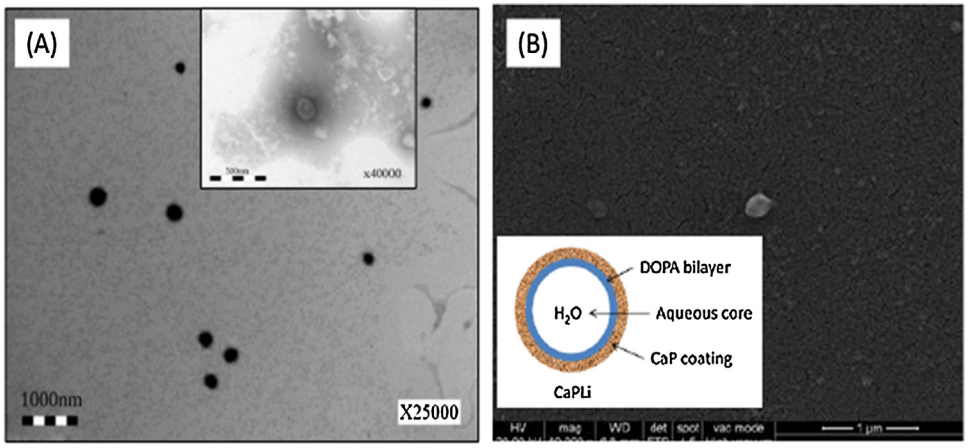

Fig. 2. (A) TEM images of CaPLi. *Inset:* TEM image of a phosphotungstic-stained CaPLi. (B) SEM image of a CaPLi. *Inset:* Schematic view of the CaPLi.

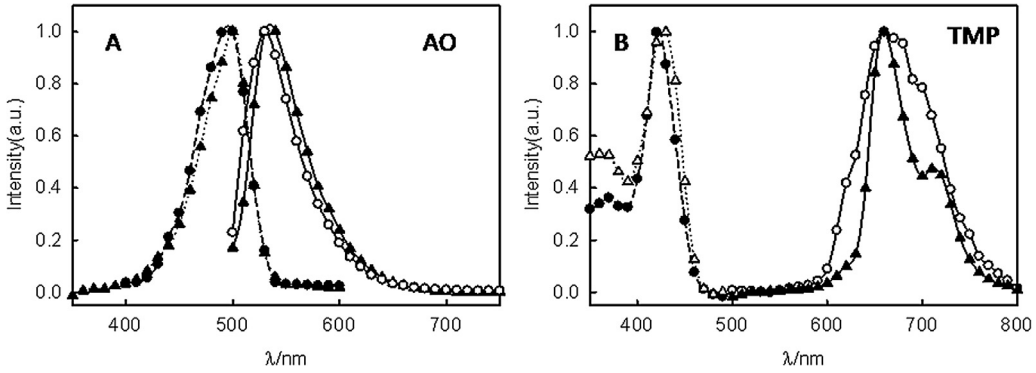

Fig. 3. Emission and excitation spectra at 296 K of aqueous solutions/suspensions of (A) AO 5×10^{-4} M (exc●, em○) and CaPLi-AO 1×10^{-3} M (excΔ, em▲). (B) 5×10^{-6} M TMP (exc●, em○) and CaPLi-TMP 1×10^{-4} M (excΔ, em▲).

According to literature reports, this red shift may be interpreted as a *red edge excitation shift effect* originated in the slow rates, relative to fluorescence lifetime, of solvent relaxation around an excited state fluorophore in organized assemblies such as the liposome [23,31]. Therefore, the presence of AO molecules interacting with the lipid vesicles is confirmed. The absence of a distinctive emission at 650 nm characteristic of AO dimmers indicates that AO entrapped in the liposome is largely a cation monomer.

The fluorescence decay of AO aqueous solutions could be well fitted to a biexponential function with fluorescence lifetime $\tau_1 = 1.6$ ns with >77% contribution to the fluorescence emission, in agreement with literature reports for the monomer emission in aqueous solutions [27]. A less significant contribution of $\tau_2 = 2.5$ ns may be assigned to AO aggregation. On the other hand, CaPLi-AO traces were well-fitted to a tri-exponential decay which includes a <1 ns lifetime attributed to the light scattering of the CaP-coated liposomes. A second lifetime, $\tau_2 = 1.8$ ns contributing to 40% of the overall fluorescence (neglecting scattering) agrees with that observed for the protonated AO in aqueous solutions, *vide supra*. The third value, $\tau_3 = 4.2$ ns contributing to 60% of the overall fluorescence is consistent with the increased lifetime decay observed for AO molecules confined in micelles [27,28,30].

Moreover,time-domain anisotropy experiments were performed for AO aqueous solutions and CaPLi-AO aqueous suspensions. The obtained anisotropy profiles could be well fitted to a single exponential, $r(t) = r_\infty + r_0 \times \exp(-t/\tau_A)$ with τ_A the correlation time, r_0 and r_∞ the initial and residual anisotropies. Since no differences were observed between r_0 (0.35 ± 0.05), r_∞ (0.06 ± 0.01), and τ_A (0.35 ± 0.02) values obtained for both samples, it is suggested that the AO molecules are not rigidly bound to the vesicles and sense similar environments within the coated liposome and in aqueous suspensions [32]. In fact, AO hydrodynamic radius obtained from the anisotropy data (7.2 ± 0.1 Å) is in agreement with the reported theoretical radius of 6.9 Å obtained using the Onsager model for solvation of a dipolar solute in a polar solvent [33]. AO is probably distributed between the aqueous phase out of the liposome and inside the liposome because a fluorescence decay characteristic of the free molecules in aqueous suspensions and a second component attributed to the interaction of the molecules with the lipid bilayer were detected. The interchange of the fluorophores between these two phases is longer than the ns time domain.

In aqueous solutions, TMP revealed excitation and emission spectra consisting in a broad band with maximum emission around 660 nm, in agreement with reported data in that solvent [34]. On the other hand, the spectrum of CaPLi-TMP shows two emission bands at 659 and 713 nm, respectively. The presence of two separated peaks was also reported for the spectrum of TMP confined in SDS micelles [34] and was assigned to TMP emission in an aqueous media and bound to the organic layer, respectively. Therefore, these observations support the confinement of TMP inside the liposomes. Also, a *red edge excitation shift effect* of 4 nm is observed for CaPLi-TMP samples (Fig. 3B) further supporting the presence of TMP molecules interacting with the lipid vesicles.

TMP in aqueous solutions shows a fluorescence decay $\tau_1 = 5.3$ ns with 70% contribution to the overall fluorescence, and a less important contribution with $\tau_1 = 1.3$ ns of unknown origin, in coincidence with reported values [26,35]. On the other hand, CaPLi-TMP traces were fitted by a tri-exponential function showing a <1 ns decay consistent with a light scattering process due to the CaP-liposomes.

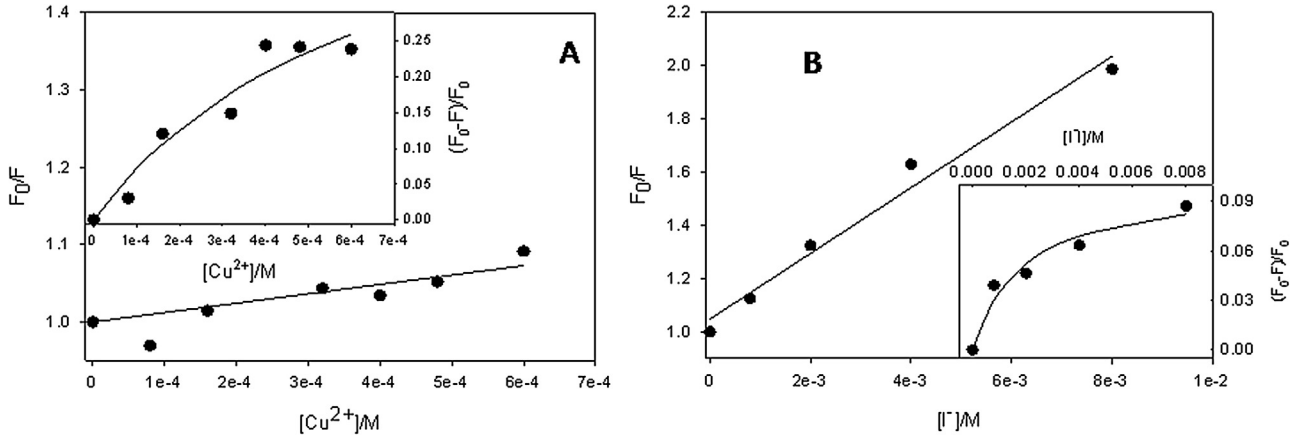

Fig. 4. (A) Stern-Volmer plot for 4×10^{-6} M AO aqueous solution. *Inset*: Modified Stern-Volmer plot $(F_0\text{-}F)/F_0$ vs $[Cu^{2+}]$/M for CaPLi-AO aqueous suspension. (B) Stern-Volmer plot for 1×10^{-5} M TMP aqueous solution. *Inset*: Modified Stern-Volmer plot $(F_0\text{-}F)/F_0$ vs $[I^-]$/M for CaPLi-TMP aqueous suspension.

$\tau_2 = 1.6$ ns with less than 1% contribution, and $\tau_3 = 8.6$ ns (responsible for the 99% of the total fluorescence) in complete agreement with the reported lifetime of TMP in phospholipid vesicles, dodecyl sulfate micelles [26], and hydrophobic solvents [34]. The obtained results clearly indicate that TMP fluorophores are almost completely inside the CaP-coated liposomes.

3.2. Quenching experiments with free flurorophores and entrapped fluorophores

To provide further evidence of the leaking of entrapped fluorophores in CaP-coated liposomes, quenching experiments were performed, both, with the free fluorophores solutions and the CaP-coated liposomes containing encapsulated fluorophores suspensions. To that purpose, the fluorescence of 4×10^{-6} M AO solutions and CaPLi-AO aqueous suspensions were quenched by the addition of different concentrations of Cu^{+2} ($\leq$60 μM) [4]. On the other hand, 1×10^{-5} M TMP aqueous solution and CaPLi-TMP aqueous suspensions were subjected to fluorescence quenching experiments by addition of $[I^-] \leq 8$ μM aqueous solutions [36].

Fig. 4A shows the diminished emission of AO and CaPLi-AO suspensions with the addition of increasing $[Cu^{2+}]$. AO fluorescence quenching in aqueous solutions follows a Stern-Volmer behavior, as plots of F_0/F linearly increase with increasing $[Cu^{2+}]$, with F_0 and F the area below AO emission curves (470–650 nm) in the absence and presence of Cu^{2+}, Fig. 4A. The slope of these plots yields the Stern-Volmer quenching constant $K_{SV} = 122 \pm 40\ M^{-1}$ which measures the degree of sensitivity of the fluorophore for the detection of the metal ion. From the latter value, the quenching bimolecular rate constant $k_q = K_{SV}/\tau_0 = (7 \pm 3) \times 10^{10}\ M^{-1}\ s^{-1}$ is calculated considering $\tau_0 = 1.6 \pm 0.1$ ns, *vide supra*. The obtained value indicates a diffusion-controlled reaction.

However, a different behavior was observed for CaPLi-AO suspensions. In this case, plots of F_0/F vs $[Cu^{2+}]$ deviate from a linear Stern-Volmer behavior, Fig. 4A *inset*. The observed deviation toward the x-axis is characteristic of systems where more than one fluorophore population is present and one this populations is not accessible to the quencher [23]. The modified form of the Stern-Volmer (Eq. (1)), describes this situation, where f_a is the fraction of accessible fluorophores and [Q] is the quencher concentration. Fitting of the data to Eq. (1) (Fig. 4A inset) yields $f_a = 0.55$ and $K_{SV} = (2000 \pm 1000)\ M^{-1}$. The 55% fraction of accessible fluorescence is in line with the fact that 40% of the total fluorescence is due to solution free AO, *vide supra*. Therefore, taking $\tau_0 = 1.8$ ns for the lifetime of the accessible fluorescence, $k_q = (1.1 \pm 0.6) \times 10^{12}\ M^{-1}\ s^{-1}$ is obtained, almost 15 times higher than the obtained value in pure aqueous solutions.

$$\frac{F_0\text{-}F}{F_0} = \frac{f_a \times K_{SV} \times [Q]}{1 + K_{SV}\,[Q]} \quad (1)$$

The enhancement in AO fluorescence quenching with Cu^{2+} in anionic SDS micellar environments is already reported in the literature and was attributed to electrostatic and steric effects on Cu^{2+} quenching introduced by the micelle surface [4]. In fact, Cu^{2+} ions quenching may take place on the surface of the CaP-coated liposomes as Cu^{2+} is well known to efficiently absorb on calcium phosphate [37]. The reaction rate constant between a reactant Q in solution and a reactant immobilized at the surface of a spherical particle L can be estimated from the Smoluchowski equation $k_{Q,AO} = 4\pi \times N R_{Q+L} D_{Q+L} \times g$ [23,38,39] where N is Avogadro's number, R_{Q+L} is the sum of the radii of quencher Q and particle L, D_{Q+L} is the mutual diffusion coefficient given by the sum of the individual coefficients and factor *g* accounts for the coulombic work needed to bring the AO molecules from the solution to the CaPLi-AO surface. Considering that the maximum adsorption of Cu^{2+} ions on hydroxyapatite is of 1.5 mg/m^2 [37], it may be expected that the surface of CaPLi-AO is well covered by adsorbed Cu^{2+} ions under the experimental conditions used in the quenching experiments. Moreover, considering the negative surface charge of CaP covered liposomes (*vide supra*), the factor *g* is expected to be >1 [40]. As a rough approximation, the individual diffusion coefficients can be estimated from the Stokes-Einstein relation [38]. Considering T = 296 K, a radius of the order of 0.7 nm for solution free AO (*vide supra*) and the range of R_L = 100–200 nm for liposomes estimated from TEM images, a diffusion rate constant $k_{Q,AO} \geq 1.5 \times 10^{12}\ M^{-1}\ s^{-1}$ is expected, of the order of the experimentally determined value, thus supporting an heterogeneous Cu^{2+} quenching process. The obtained results strongly suggest that AO may partly diffuse out of the CaPLi-AO and the quenching takes place on the liposome outer layer.

The fluorescence quenching of TMP aqueous solutions by iodide anions also yield straight plots of F_0/F *vs.* $[I^-]$. The slope of the plot yields the Stern-Volmer quenching constant $K_{SV} = 130 \pm 10\ M^{-1}$. Considering $\tau_0 = 5.3$ ns, *vide supra*, a diffusion-controlled bimolecular quenching rate constant $k_q = K_{SV}/\tau_0 = (2.5 \pm 0.9) \times 10^{10}\ M^{-1}\ s^{-1}$ is obtained. However, quenching experiments with CaPLi-TMP aqueous suspensions also deviate from a linear Stern-Volmer behavior. The data shown in Fig. 4B *inset* can be well fitted to the modified Stern-Volmer equation (Eq. (1)) considering the fraction of accessible fluorophores $f_a = 0.1$ and $K_{SV} = 500 \pm 200\ M^{-1}$. The small fraction of accessible fluorophores is in accordance with the fact that less than 1% of the total fluorescence is due to

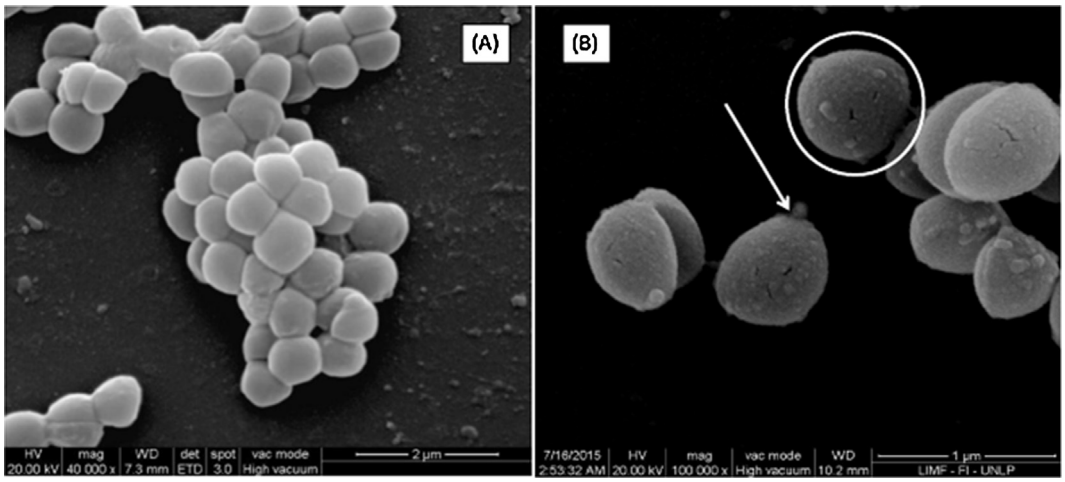

Fig. 5. Scanning electron microscopy images of (A) *S. aureus* biofilm incubated for 15 min without liposomes and (B) *S. aureus* biofilm incubated for 15 min with CaPLi-AO. The arrow show a CaP-coated liposome in close proximity of the bacteria cell.

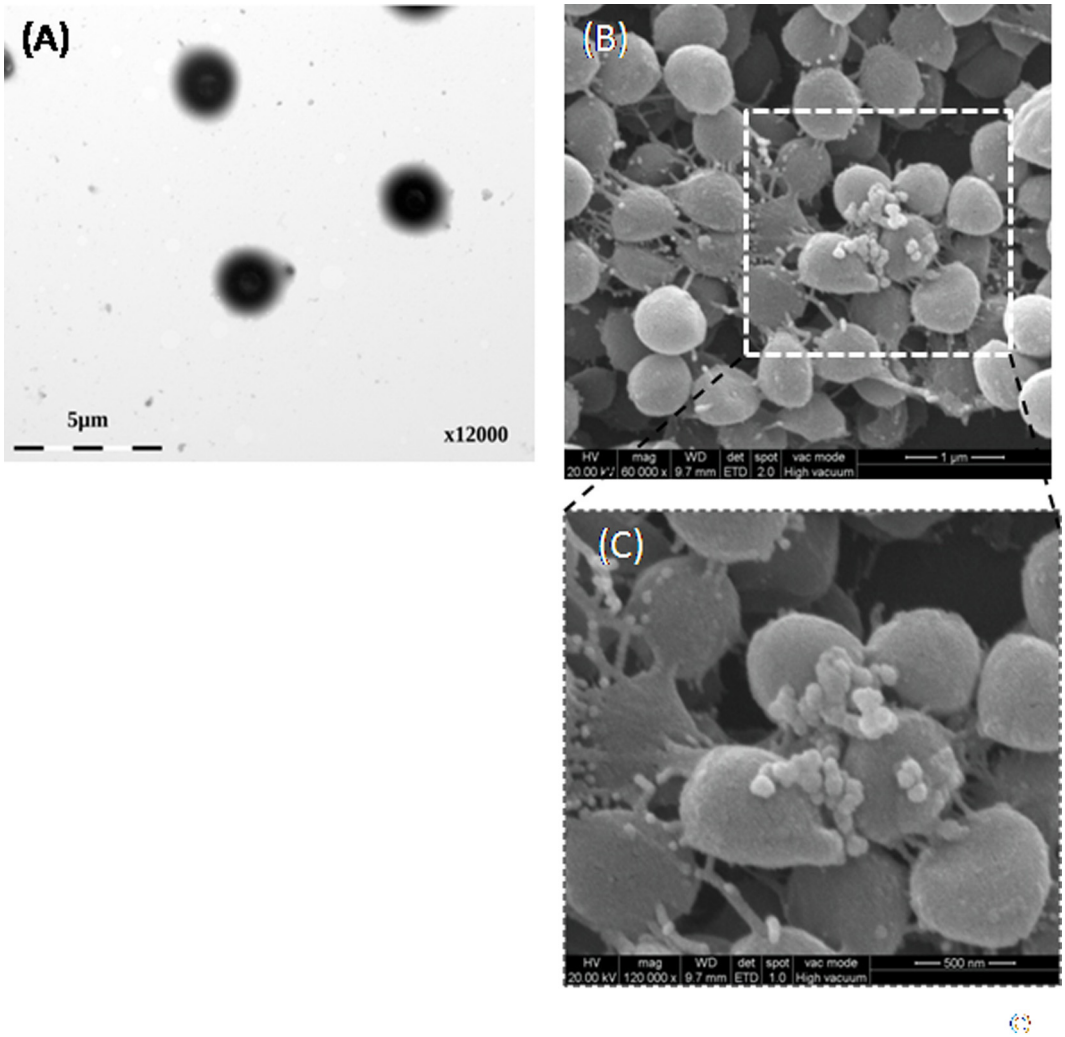

Fig. 6. Microscopy images of *S. aureus* cultures after 2 h incubation in the presence of CaPLi-AO. (A) TEM. (B) and (C) SEM micrographs.

solution-free TMP, *vide supra*. In addition, taking $\tau_0 = 5.3$ ns for the lifetime of the accessible fluorescence, $k_q = (9.4 \pm 0.3) \times 10^{10}\ M^{-1} s^{-1}$ is obtained, on the order of the value calculated in aqueous solutions. It is interesting to note that, the fluorescence experiments strongly evidenced the negligible diffusion of TMP molecules out of CaPLi-TMP, in contrast with the partial diffusion observed for AO molecules, probably due to the higher porphyrin radius of 1 nm [41].

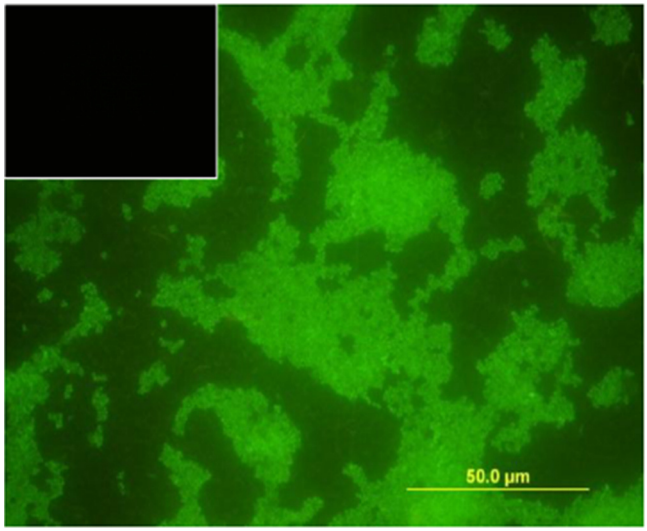

Fig. 7. *S. aureus* biofilm incubated for 2 h with CaPLi-AO. *Inset*: Luminescence of CaPLi-AO deposited on glass slides as observed in the epifluorescence microscope under identical excitation and emission detection conditions.

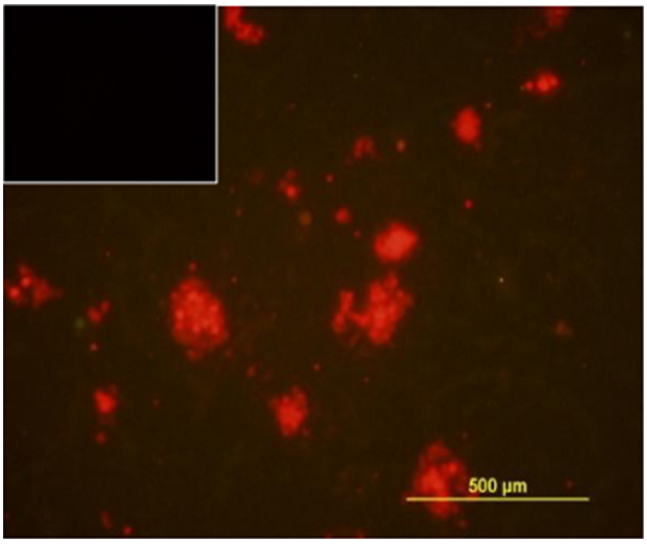

Fig. 8. Smears of *S. aureus* incubated for 2 h with CaPLi-TMP. *Inset*: Luminescence of CaPLi-TMP deposited on glass slides as observed in the epifluorescence microscope under identical excitation and emission detection conditions.

3.3. Interaction between CaP-coated liposomes and bacteria

The MICs of free and CaP liposomal-entrapped fluorophores AO and TMP, obtained for *S. aureus* were comparable. Bacterial growth was observed in all cases and no toxicity was detected in concentrations up to 10^{-4}–10^{-5} M for all samples. The assays were perfomed in the dark, avoiding any photodynamic activity of TMP. The low toxicity of CaP nanoparticles against *S. aureus* correlates with literature reports [42].

In order to analyze the liposome-bacteria interaction under different bacterial lifestyles, *S. aureus* was grown as free-living planktonic cells and biofilms. Bacterial cultures were visualizated by SEM and TEM techniques. Microscopy images of *S. aureus* culture incubated in the absence and presence of CaPLi-AO for 15 min and 2 h at 37 °C are shown in Figs. 5 and 6 respectively. The SEM image in Fig. 5A shows the smooth surface of bacteria incubated without CaPLi. Fig. 5B obtained for a sample incubated during 15 min shows a high ratio of CaPLi-AO/bacteria and a very good adhesion of the liposomes to the cells, as they were not removed by the treatment previous to SEM microscopy (see Section 2). A detailed observation of the image gives evidence of a rough surface and the adsorption of the liposomes on the bacterial surface. Thus, strongly suggesting that adhesion of the CaPLi-AO into the bacterial cell is a plausible process.

After 2 h incubation, TEM images in Fig. 6A show a low ratio of liposomes adjacent to the bacterial cells. Corresponding SEM images show a young biofilm with extracellular polymeric matrix strands connecting the cells (see Fig. 6B and C). CaPLi-AO placed over bacteria surfaces is clearly noticed in Fig. 6B and the expansion of the latter, Fig. 6C. Agglomeration of the liposomes was observed in Fig. 6B, however, the images indicate that the morphology of the bacteria was not affected by the presence of the CaPLi-AO. Additionally, the presence of rod-like nanoparticles observed in SEM images in the presence of bacterial cells is attributed to CaP crystal (see Supplementary Material).

S. aureus biofilms inoculated with CaPLi-AO and *S. aureus* smears inoculated with CaPLi-TMP for 2 h were also observed in a fluorescence microscope after buffer washing, Figs. 7 and 8, respectively. The negligible emission of CaPLi-AO and CaPLi-TMP suspension deposited on glass slides is also shown for comparison.

Many properties of aggregates resemble those of biofilms including tolerance to hazardous environments [43]. Accordingly, Miñan et al. reported that aggregation of *S. aureus* sessile cells is responsible of the increase in the antibiotic resistance [44]. Additionally, it was proposed for another opportunistic pathogen, *P. aeruginosa*, that non-attached planktonic aggregates of cells may be considered dispersed biofilms [45] and that these planktonic aggregates have the same protective properties as biofilms. Considering these similarities it may be assumed that the response of aggregates of the smear and biofilms (Figs. 7 and 8) to CaPLi-AO or CaPLi-TMP environment is similar.

Fig. 7 shows aggregates characteristic of *S. aureus* biofilms with a good adhesion to the glass slide surface and optimal bacterial staining, as well as cells morphology conservation. The green emission of CaPLi-AO stained *S. aureus* samples observed is characteristic of the monomeric dye in solution [46]. Conversely, no significant fluorescence is observed from CaPLi-AO deposited on the glass slides under similar excitation and detection conditions. Consequently, the good staining of *S. aureus* biofilms herein observed 2 h after the addition of CaPLi-AO, clearly suggests the diffusion of AO out of the adsorbed CaPLi-AO on the bacteria cell wall. In fact, the cells were not significantly stained immediately after the inoculation of the biofilms with CaPLi-AO, thus strongly suggesting a slow AO releasing process.

According to photophysical data c.a. 40% of AO is released to the outer solution while only a small percentage of TMP is observed to reach the outer liposome surface. Surprisingly, a notable TMP staining of bacterial smears after two hours inoculation with CaPLi-TMP (Fig. 8) was observed, despite TMP diffusion out of the CaPLi-TMP is of no significance. Therefore, the optimal staining of bacteria by CaPLi-TMP seems to involve a fast release of TMP as a consequence of the CaPLi-TMP/bacteria cell interaction. Such interaction might involve a complex process leading to the partial destruction of the CaP shell thus promoting an efficient transport of TMP out of the nanoparticle.

It is reported in literature that, the adherence [47] and fusion [48] of liposomal vesicles with the peptidoglycan barrier of Gram-positive bacteria could lead to the release of liposomal content close to the cytoplasmic membrane and increased intracellular drug concentration. Moreover, the interaction of different phases of CaP with *S. aureus* biofilm is well reported in the literature [49,50]. Schwiertz and coworkers suggested the incorporation of polymer coated CaP nanoparticles of 50–100 nm size to *S. aureus* [42]. Moreover, *S. aureus*, being Gram-positive, possesses a cell wall of about

25 nm thick [51], of alternating phosphate and ribitol (wall teichoic acids) or glycerol (lipoteichoic acids) groups [52,53]. Also, calcium and magnesium are the major endogeneous metals found in the cell wall of Gram-positive bacteria [51]. Results from this author provided microbiological evidence that showed phosphates interacted with *S. aureus* cell wall by a metal chelation mechanism. The internalization of CaP crystal growing within the bacterial matrix was proposed to be responsible of an increased volume within the bacteria [54]. Therefore, the evidence in the literature supports that CaP coating of the liposomes may be the main factor affecting the surface interaction and probably the internalization on *S. aureus*.

Since the observed TMP staining process takes place only in contact with the bacterial cell wall, CaP-coated liposomes are a potential drug delivery agent for *S. aureus* cell targets. On this respect, it is well known that porphyrins are efficient singlet oxygen photosensitizers for photodynamic bacteria killing [55,56]. Therefore, CaPLi-TMP and CaPLi-containing TMP related molecules may be used as specific drugs for *S. aureus* photoinactivation treatment.

4. Conclusions

CaP-coated liposomes containing fluorophores were successfully synthesized by DOPA lipid extrusion and subsequent CaP deposition over liposome templates. The thickness of the CaP shell was controlled by the CEPA addition time. The liposomes gained stability after coating, as can be seen by SEM images. Distribution of the AO and TMP molecules in the surrounding aqueous phase and the liposomes was demonstrated by the shifts and broadening in excitation–emission matrices and the modified Stern-Volmer model for fluorescence quenching. The fluorescence experiments strongly evidenced the negligible diffusion of TMP molecules out of CaP-coated liposomes, in contrast with the partial diffusion observed for AO molecules.

A close interaction between liposomes and *S. aureus* biofilm was evidenced by TEM and SEM assays. The CaP-coated lipidic vesicles remained adhered to the bacterial surface even after intense washing treatment. The staining of smears was effectively accomplished by CaPLi-TMP despite TMP diffusion out of the CaP-coated liposomes is an extremely slow process. The latter observation strongly suggests that CaP-coated liposomes interaction with the bacteria cell wall disrupts the CaP shell releasing TMP. In that scenario, the diffusion of fluorophore from the CaP-coated liposomes through the bacterial membrane can provide a sustained drug delivery system to control *S. aureus* biofilm growth.

Conflict of interest

The authors declare no competing financial interest.

Acknowledgments

M.L.D, M.F.L.M., M.C.G. and A.M. are research members of CONICET, Argentina. This research was supported by the grant PICT 2012-2359 and PICT 2012-1775 from ANPCyT, PIP0771 from CONICET and UNLP I173 from University of La Plata.

Appendix A. Supplementary data

Supplementary data associated with this article can be found, in the online version, at http://dx.doi.org/10.1016/j.colsurfb.2016.03.003.

References

[1] A.K. Singh, P.K. Kilpatrick, R.G. Carbonell, Application of antibody and fluorophore-derivatized liposomes to heterogeneous immunoassays for d-dimer, Biotechnol. Prog. 12 (1996) 272–280.
[2] K.P. McNamara, Z. Rosenzweig, Dye-encapsulating liposomes as fluorescence-based oxygen nanosensors, Anal. Chem. 70 (1998) 4853–4859.
[3] J.E. Schroeder, I. Shweky, H. Shmeeda, U. Banin, A. Gabizon, Folate-mediated tumor cell uptake of quantum dots entrapped in lipid nanoparticles, J. Control. Release 124 (2007) 28–34.
[4] A.K. Ghosh, A. Samanta, P. Bandyopadhyay, Cu^{2+}-Induced micellar charge selective fluorescence response of acridine orange: effect of micellar charge, pH, and mechanism, J. Phys. Chem. B 115 (2011) 11823–11830.
[5] J.O. Eloy, M.C. de Souza, R. Petrilli, J.P.A. Barcellos, R.J. Lee, J.M. Marchetti, Liposomes as carriers of hydrophilic small molecule drugs: strategies to enhance encapsulation and delivery, Colloids Surf. B Biointerfaces 123 (2014) 345–363.
[6] J. Ha, S.K. Cho, E.S. Park, K. Han, H.D. Han, B.C. Shin, Enhanced stability of hydroxyapatite-coated liposomes for ultrasound-triggered drug release, Bull. Korean Chem. Soc. 36 (2015) 83–87.
[7] Y. Dong, P. Dong, D. Huang, L. Mei, Y. Xia, Z. Wang, et al., Fabrication and characterization of silk fibroin-coated liposomes for ocular drug delivery, Eur. J. Pharm. Biopharm. 91 (2015) 82–90.
[8] K. Kawakami, Y. Nishihara, K. Hirano, Effect of hydrophilic polymers on physical stability of liposome dispersions, J. Phys. Chem. B. 105 (2001) 2374–2385.
[9] H.T. Schmidt, B.L. Gray, P.A. Wingert, A.E. Ostafin, Assembly of aqueous-cored calcium phosphate nanoparticles for drug delivery, Chem. Mater. 16 (2004) 4942–4947.
[10] C.-H. Yeo, S.H.S. Zein, A.L. Ahmad, D.S. McPhail, Comparison of DOPA and DPPA liposome templates for the synthesis of calcium phosphate nanoshells, Ceram. Int. 38 (2012) 561–570.
[11] S.N. Park, N.R. Jo, S.H. Jeon, Chitosan-coated liposomes for enhanced skin permeation of resveratrol, J. Ind. Eng. Chem. 20 (2014) 1481–1485.
[12] S. Nguyen, M. Adamczak, M. Hiorth, G. Smistad, H.M. Kopperud, Interactions of liposomes with dental restorative materials, Colloids Surf. B Biointerfaces 136 (2015) 744–751.
[13] S. Sharma, A. Verma, B.V. Teja, G. Pandey, N. Mittapelly, R. Trivedi, et al., An insight into functionalized calcium based inorganic nanomaterials in biomedicine: trends and transitions, Colloids Surf. B Biointerfaces 133 (2015) 120–139.
[14] P.A. Wingert, H. Mizukami, A.E. Ostafin, Enhanced chemiluminescent resonance energy transfer in hollow calcium phosphate nanoreactors and the detection of hydrogen peroxide, Nanotechnology 18 (2007) 295707.
[15] Z. Darzynkiewicz, Chapter 27 differential staining of DNA and RNA in intact cells and isolated cell nuclei with acridine orange, in: D. Zbigniew, A.C. Harry (Eds.), Methods Cell Biol., Academic Press, 1990, pp. 285–298.
[16] S. Clerc, Y. Barenholz, A quantitative model for using acridine orange as a transmembrane pH gradient probe, Anal. Biochem. 259 (1998) 104–111.
[17] J.W. Snyder, J.D.C. Lambert, P.R. Ogilby, 5,10,15,20-Tetrakis(*N*-Methyl-4-Pyridyl)-21*H*,23*H*-porphine (TMPyP) as a sensitizer for singlet oxygen imaging in cells: characterizing the irradiation-dependent behavior of TMPyP in a single cell, Photochem. Photobiol. 82 (2006) 177–184.
[18] F. Wilkinson, W.P. Helman, A.B. Ross, Quantum yields for the photosensitized formation of the lowest electronically excited singlet state of molecular oxygen in solution, J. Phys. Chem. Ref. Data 22 (1993) 113–262.
[19] S. Ferro, F. Ricchelli, G. Mancini, G. Tognon, G. Jori, Inactivation of methicillin-resistant *Staphylococcus aureus* (MRSA) by liposome-delivered photosensitising agents, J. Photochem. Photobiol. B Biol. 83 (2006) 98–104.
[20] D. Dong, N. Thomas, B. Thierry, S. Vreugde, C.A. Prestidge, P.-J. Wormald, Distribution and inhibition of liposomes on *Staphylococcus aureus* and *Pseudomonas aeruginosa* biofilm, PLoS One 10 (2015) e0131806.
[21] D.P. Calfee, C.D. Salgado, A.M. Milstone, A.D. Harris, D.T. Kuhar, J. Moody, et al., Strategies to prevent methicillin-resistant *Staphylococcus aureus* transmission and infection in acute care hospitals: 2014 update, Infect. Control Hosp. Epidemiol. 35 (2014) 772–796.
[22] P. Wayne, Performance Standards for Antimicrobial Susceptibility Testing; Approved Standard, 8th ed., Clinical and Laboratory Standards Institute, 2009 (Do).
[23] J.R. Lakowicz, Principles of Fluorescence Spectroscopy, 3rd ed., Springer, New York, 2006.
[24] M. Talbot, R. White, Methanol fixation of plant tissue for Scanning Electron Microscopy improves preservation of tissue morphology and dimensions, Plant Methods 9 (2013) 36.
[25] N. Berger, A. Sachse, J. Bender, R. Schubert, M. Brandl, Filter extrusion of liposomes using different devices: comparison of liposome size, encapsulation efficiency, and process characteristics, Int. J. Pharm. 223 (2001) 55–68.
[26] D. de Sousa Neto, A. Hawe, M. Tabak, Interaction of meso-tetrakis (4-*N*-methylpyridyl) porphyrin in its free base and as a Zn(II) derivative with large unilamellar phospholipid vesicles, Eur. Biophys. J. 42 (2013) 267–279.
[27] R.D. Falcone, N.M. Correa, M.A. Biasutti, J.J. Silber, Acid-base and aggregation processes of acridine orange base in *n*-heptane/AOT/water reverse micelles, Langmuir 18 (2002) 2039–2047.
[28] A.K. Shaw, S.K. Pal, Fluorescence relaxation dynamics of acridine orange in nanosized micellar systems and DNA, J. Phys. Chem. B 111 (2007) 4189–4199.

[29] A.K. Ghosh, A. Samanta, P. Bandyopadhyay, Anionic micelle-induced fluorescent sensor activity enhancement of acridine orange: mechanism and pH effect, Chem. Phys. Lett. 507 (2011) 162–167.
[30] N. Miyoshi, K. Hara, I. Yokoyama, G. Tomita, M. Fukuda, Fluorescence lifetime of acridine orange in sodium dodecyl sulfate premicellar solutions, Photochem. Photobiol. 47 (1988) 685–688.
[31] A. Chattopadhyay, S. Haldar, Dynamic insight into protein structure utilizing red edge excitation shift, Acc. Chem. Res. 47 (2014) 12–19.
[32] L. Frauchiger, H. Shirota, K.E. Uhrich, E.W. Castner, Dynamic fluorescence probing of the local environments within amphiphilic starlike macromolecules, J. Phys. Chem. B 106 (2002) 7463–7468.
[33] V.K. Sharma, P.D. Sahare, R.C. Rastogi, S.K. Ghoshal, D. Mohan, Excited state characteristics of acridine dyes: acriflavine and acridine orange, Spectrochim. Acta A Mol. Biomol. Spectrosc. 59 (2003) 1799–1804.
[34] P.J. Gonçalves, P.L. Franzen, D.S. Correa, L.M. Almeida, M. Takara, A.S. Ito, et al., Effects of environment on the photophysical characteristics of mesotetrakis methylpyridiniumyl porphyrin (TMPyP), Spectrochim. Acta A Mol. Biomol. Spectrosc. 79 (2011) 1532–1539.
[35] I.V. Sazanovich, E.P. Petrov, V.S. Chirvony, Interaction of cationic 5,10,15,20-tetrakis(4-*N*-methyl pyridyl) porphyrin with mono- and polynucleotides: a study by picosecond fluorescence spectroscopy, Opt. Spectrosc. 100 (2006) 209–218.
[36] I. Bronshtein, M. Afri, H. Weitman, A.A. Frimer, K.M. Smith, B. Ehrenberg, Porphyrin depth in lipid bilayers as determined by iodide and parallax fluorescence quenching methods and its effect on photosensitizing efficiency, Biophys. J. 87 (2004) 1155–1164.
[37] D.F. Mercado, G. Magnacca, M. Malandrino, A. Rubert, E. Montoneri, C. Gonzalez, Paramagnetic iron-doped hydroxyapatite nanoparticles with improved metal sorption properties, ACS Appl. Mater. Interfaces 6 (2014) 3937–3946.
[38] A. Nag, A.R. Dinner, Enhancement of diffusion-controlled reaction rates by surface-induced orientational restriction, Biophys. J. 90 (2006) 896–902.
[39] P. Caregnato, S.G. Bertolotti, M.C. Gonzalez, D.O. Mártire, Water/silica nanoparticle interfacial kinetics of sulfate hydrogen phosphate, and dithiocyanate radicals, Photochem. Photobiol. 81 (2005) 1526–1533.
[40] P. Caregnato, M.D.E. Forbes, D.B. Soria, D.O. Maírtire, M.C. Gonzalez, Chemisorbed thiols on silica particles: characterization of reactive sulfur species, J. Phys. Chem. C 114 (2010) 5080–5087.
[41] S.M. Aly, G.H. Ahmed, B.S. Shaheen, J. Sun, O.F. Mohammed, Molecular-structure control of ultrafast electron injection at cationic porphyrin–CdTe quantum dot interfaces, J. Phys. Chem. Lett. 6 (2015) 791–795.
[42] J. Schwiertz, A. Wiehe, S. Gräfe, B. Gitter, M. Epple, Calcium phosphate nanoparticles as efficient carriers for photodynamic therapy against cells and bacteria, Biomaterials 30 (2009) 3324–3331.
[43] J. Haaber, M.T. Cohn, D. Frees, T.J. Andersen, H. Ingmer, Planktonic aggregates of *Staphylococcus aureus* protect against common antibiotics, PLoS One 7 (2012) e41075.
[44] A. Miñán, P.L. Schilardi, M.F.L. de Mele, The importance of 2D aggregates on the antimicrobial resistance of *Staphylococcus aureus* sessile bacteria, Mater. Sci. Eng. C 61 (2016) 199–206.
[45] M. Alhede, K.N. Kragh, K. Qvortrup, M. Allesen-Holm, M. van Gennip, L.D. Christensen, et al., Phenotypes of non-attached *Pseudomonas aeruginosa* aggregates resemble surface attached biofilm, PLoS One 6 (2011) e27943.
[46] L. Netuschil, T. Auschill, A. Sculean, N. Arweiler, Confusion over live/dead stainings for the detection of vital microorganisms in oral biofilms—which stain is suitable? BMC Oral Health 14 (2014) 2.
[47] P.M. Furneri, M. Fresta, G. Puglisi, G. Tempera, Ofloxacin-loaded liposomes in vitro activity and drug accumulation in bacteria, Antimicrob. Agents Chemother. 44 (2000) 2458–2464.
[48] K. Banerjee, S. Banerjee, S. Das, M. Mandal, Probing the potential of apigenin liposomes in enhancing bacterial membrane perturbation and integrity loss, J. Colloid Interface Sci. 453 (2015) 48–59.
[49] V. Uskoković, T.A. Desai, Simultaneous bactericidal and osteogenic effect of nanoparticulate calcium phosphate powders loaded with clindamycin on osteoblasts infected with *Staphylococcus aureus*, Mater. Sci. Eng. C 37 (2014) 210–222.
[50] U. Furustrand Tafin, B. Betrisey, M. Bohner, T. Ilchmann, A. Trampuz, M. Clauss, Staphylococcal biofilm formation on the surface of three different calcium phosphate bone grafts: a qualitative and quantitative in vivo analysis, J. Mater. Sci. Mater. Med. 26 (2015) 1–8.
[51] R. Lee, Antibacterial Mechanism of Phosphates in *Staphylococcus Aureus*, Retrosp. Theses Diss., Iowa State University, 1993 http://lib.dr.iastate.edu/rtd/10246.
[52] K. Dillen, C. Bridts, P. Van der Veken, P. Cos, J. Vandervoort, K. Augustyns, et al., Adhesion of {PLGA} or Eudragit®/PLGA nanoparticles to *Staphylococcus* and *Pseudomonas*, Int. J. Pharm. 349 (2008) 234–240.
[53] M. Gross, S.E. Cramton, F. Götz, A. Peschel, Key role of teichoic acid net charge in *Staphylococcus aureus* colonization of artificial surfaces, Infect. Immun. 69 (2001) 3423–3426.
[54] C.K. Arellano, The Calcification of *Staphylococcus Aureus* Bacteria: a Potential Defense Mechanism Against Infections, Master Theses, University of California, 2010.
[55] G. Rossi, D. Goi, C. Comuzzi, The photodynamic inactivation of Staphylococcus aureus in water using visible light with a new expanded porphyrin, J. Water Health 10 (2012) 390–399.
[56] A. Hanakova, K. Bogdanova, K. Tomankova, K. Pizova, J. Malohlava, S. Binder, et al., The application of antimicrobial photodynamic therapy on *S. aureus* and *E. coli* using porphyrin photosensitizers bound to cyclodextrin, Microbiol. Res. 169 (2014) 163–170.